UNIVERSITY OF LATVIA
FACULTY OF PHYSICS AND MATHEMATICS

Andris Antuzevičs

LOCAL STRUCTURE OF S-STATE RARE EARTH IONS IN FLUORIDES AND OXYFLUORIDE GLASS CERAMICS

SUMMARY OF DOCTORAL THESIS

Submitted for the Degree of Doctor of Physics
Subfield of Solid State Physics

Riga, 2017

The doctoral thesis was carried out at the Institute of Solid State Physics, University of Latvia from 2014 to 2017.

The thesis contains an introduction, 4 chapters, conclusions and a reference list.

Type of thesis: dissertation in physics in the subfield of solid state physics.

Supervisor:
Dr. habil. phys. **Uldis Rogulis**, professor, University of Latvia.

Reviewers:
1) *Dr. habil. phys.* **Linards Skuja**, senior researcher, Institute of Solid State Physics, University of Latvia;
2) *Dr. habil. phys.* **Jurijs Dehtjars**, professor, Riga Technical University;
3) *Dr. Sci.* **Aleksandr Lushchik**, professor, University of Tartu.

The thesis will be defended at the public session of the Doctoral Committee of Physics, Astronomy and Mechanics, University of Latvia at 11:00 on 12th of December, 2017 in auditorium No. 233 of the Faculty of Physics and Mathematics, University of Latvia, Zellu street 25, Riga.

The thesis and its summary is available at the Library of the University of Latvia, Kalpaka blvd. 4, Riga.

Chairman of the Doctoral Comittee _____ *Dr. habil. phys.* **Linards Skuja**

Secretary of the Doctoral Comittee _____ **Laureta Buševica**

ISBN 978-9934-18-288-4

ABSTRACT

In this work local structure of S-state rare earth ions (Gd^{3+} and Eu^{2+}) is investigated with electron paramagnetic resonance (EPR) spectroscopy technique in ScF_3 and BaY_2F_8 single crystals as well as in oxyfluoride glass ceramics containing MeF_2 (Me = Ca, Ba, Sr) crystallites.

EPR spectra parameters at different temperatures for gadolinium in ScF_3 – crystal with negative thermal expansion coefficient – indicate a positive expansion of the centre local structure with temperature. The Gd^{3+} centre of BaY_2F_8 crystal can be described with a set of low symmetry EPR spectra parameters.

As S-state ions embed the crystalline phase of oxyfluoride glass ceramics, the glassy U-type spectrum is superimposed by an intensive EPR spectra fine structure at g = 1.99. Good agreement between the experimental and simulated spectra can be achieved by taking the defect centre parameters of the corresponding single crystals. EPR spectra of glass ceramics with europium contain information about the valence state of ions as well as Eu^{2+} local structure.

TABLE OF CONTENTS

1. INTRODUCTION

1.1. Motivation

One of the main motivations for the study of solid state physics is the fact that understanding of microscopic structure and properties is the foundation of modern technology. In many applications, for example, solid state lasers, scintillators, luminescent coatings etc. the host material has to be doped with impurities to ensure the desired optical properties. Fluoride crystals are exceptionally suitable hosts for rare earth activators in optical applications because the low probability of nonradiative transitions can lead to a highly efficient luminescence. The studied BaY_2F_8 crystal is a well-known solid state laser host material. Currently erbium doped BaY_2F_8 is also being studied as a coating for solar cell efficiency improvement. Doped oxyfluoride glass ceramics, on the other hand, are a promising alternative to the currently used phosphors in white light emitting diodes. In addition to good optical properties, ScF_3 is special with a pronounced negative thermal expansion coefficient, therefore, structural studies of this crystal are of fundamental interest.

For a complete characterization of doped materials, the conventional X-ray diffraction and electron microscopy methods need to be supplemented with methods that yield information about activator local structure. The local electronic structure of point defects can be studied with absorption spectroscopy methods by measuring the attenuation of electromagnetic radiation as it passes through the sample. For the study of paramagnetic centres (ions, which have an uncompensated spin in the outer electron shell) magnetic resonance spectroscopy techniques are extremely useful because they give detailed information about the defect structure and interactions with the local environment.

Paramagnetic probes that are sensitive to the degree of order in the solid and crystalline field symmetry as well as surrounding elements and the nature of chemical bonds between them must be chosen for the study of local structure. Effective spin $S = 7/2$ ions Gd^{3+} and Eu^{2+} are exceptionally suitable probes because the nature of electron paramagnetic resonance fine structure is determined by the host material.

In present work the incorporation of gadolinium in ScF_3 and BaY_2F_8 single crystals is studied as well as the Gd^{3+} and Eu^{2+} ion structure is systematically characterized in oxyfluoride glass ceramics, which contain fluorite structure (CaF_2, BaF_2, SrF_2) crystallites.

1.2. Aim and objectives of the work

The aim of this work is the characterization of activator local structure in perspective fluoride crystals and oxyfluoride glass ceramics with electron paramagnetic resonance (EPR) spectroscopy and $S = 7/2$ ion (Gd^{3+}, Eu^{2+}) paramagnetic probes.

Objectives for the realization of the aim are:

- systematic EPR spectra measurements in the studied samples;
- parameterization, simulation and interpretation of the EPR spectra;
- characterization of sample structure with X-ray diffraction, X-ray fluorescence and transmission electron microscopy measurements;
- study of optical properties with photoluminescence, absorption and transmission measurement techniques.

1.3. Scientific novelty of the work

The results of these studies are novel and have been published in international journals. For the first time, the results have allowed to:

- identify a Gd^{3+} centre in BaY_2F_8;
- determine EPR spectra parameters at different temperatures for Gd^{3+} centre in ScF_3 – crystal with negative thermal expansion coefficient;
- characterize the incorporation of gadolinium in the fluorite structure (CaF_2, SrF_2, BaF_2) crystalline phase of oxyfluoride glass ceramics;
- detect previously unreported Eu^{2+} centres in glass ceramics.

1.4. Author's contribution

Experimental measurements have been performed in the Institute of Solid State Physics, University of Latvia (LU ISSP). The author has done all the experimental EPR spectra measurements and simulations as well as differential thermal analysis (DTA), X-ray fluorescence (XRF), transmittance and absorption measurements. The author is responsible for the processing and interpretation of all data presented here and for four publications is the main and corresponding author.

X-ray diffraction (XRD) measurements have been made by Reinis Ignatans and transmission electron microscopy (TEM) images have been prepared by Dr. Krisjanis Smits. The glass samples were made by Meldra Kemere.

2. LITERATURE REVIEW

2.1. Electron paramagnetic resonance

Electron paramagnetic resonance (EPR) is a field of spectroscopy, which studies systems with unpaired electrons. Splitting of electron spin states can be observed if such system is introduced to external magnetic field. It is possible to induce a transition from one spin state to another by applying electromagnetic radiation with suitable energy and observe a (radiation absorbtion) resonance. A similar principle is used in the widely applied nuclear magnetic resonance technique in medicine, where the spin states of nuclei are split instead of electrons'. The number, positions and intensities of EPR spectra lines are dependent not only on the system, but also the host material, therefore, EPR is exceptionally suitable for the study of paramagnetic centre local structure.

2.1.1. Zeeman effect

The quantum nature of the electron determines that besides the orbital angular momentum it possesses an internal angular momentum associated with its spin. If electron's orbital movement can be imagined as a current flowing in a closed circuit then for spin phenomenon a classical analogue has not been discovered yet. In classical and quantum physics angular momentum J is proportional to magnetic moment:

$$\mu = \gamma J \tag{1}$$

where γ – the gyromagnetic ratio. [1] When magnetic moment is placed in external magnetic field B, it acquires additional potential energy:

$$U = -\mu B \tag{2}$$

As a consequence of spin state quantization, the energy levels of magnetic dipole in external magnetic field can also only possess discrete values. The energy difference between states with quantum numbers M_S = ± 1/2 in magnetic field is:

$$\Delta U = U_{M_S=1/2} - U_{M_S=-1/2} = g_e \mu_B B \tag{3}$$

The proportionality coefficient μ_B is called the Bohr Magneton and g – the Zeeman spectroscopic splitting factor ($g_e \approx 2.0023$). Figure 2.1 shows Zeeman effect of a free electron – spin state with $M_S = \pm 1/2$ linear energy dependence on the magnetic field value. By choosing electromagnetic radiation with appropriate energy and frequency ν, it is possible to excite $M_S = -1/2 \rightarrow M_S = +1/2$ transition and observe electron paramagnetic resonance:

$$h\nu = g_e \mu_B B \tag{4}$$

EPR spectrum is usually recorded as the first derivative of microwave radiation absorption, which is achieved by magnetic field modulation in small amplitude. During a conventional EPR experiment a constant frequency continuous wave microware radiation is applied while magnetic field is increased linearly. From equation (4) it can be estimated, that for typical X-band microwaves with $\nu \approx 9$ GHz, the resonance field will be at $B \approx 0.3$ T = 3000 G, which translates to energy difference between spin states a few hundredth of a meV. [1]

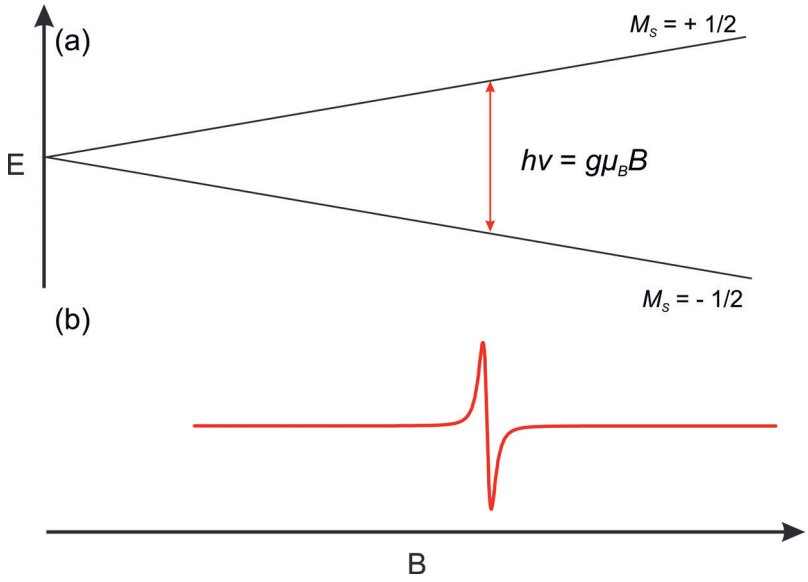

Fig. 2.1. **(a) Spin state splitting of a free electron in external magnetic field and (b) the corresponding EPR spectrum.**

2.1.2. Spin-Hamiltonian formalism

As seen in figure 2.1, for paramagnetic centres, which interact only with external magnetic field, the EPR spectra consist of 1 resonance line. Information to be gained from such spectrum is rather limited – one could calculate the spectroscopic splitting factor for the defect, but it would difficult to judge the defect structure and interactions with surroundings. Fortunately EPR spectra in solids often form complex signals which contain information about the interactions between the paramagnetic centre and crystalline electric field as well as the local magnetic fields created by the surrounding magnetic dipoles.

It is too complicated to analyse EPR spectra of impurity ions by seeking a precise Schrodinger equation solution. Therefore, experimental resonance positions are calculated using spin-Hamiltonian (SH) formalism, which contains only electron and nuclear spin interactions and appropriate SH parameters. The different interactions of the paramagnetic centre can be written separately:

$$\hat{H} = \hat{H}_{EZ} + \hat{H}_{ZFS} + \hat{H}_{HFS} + \ldots \tag{5}$$

where $\hat{H}_{EZ}$ – electron Zeeman interaction; $\hat{H}_{ZFS}$ – EPR spectra fine structure interaction; $\hat{H}_{HFS}$ – EPR spectra hyperfine structure.

If the studied sample contains two or more unpaired electrons which are bound too close to treat their magnetic moments separately, the centre must be described with an effective spin S greater than 1/2. Spin-orbital interactions of magnetic moments and electron dipole interactions appear as additional EPR spectra fine structure in these systems. Fundamental distinction of fine structure from other SH interactions is that electronic states are split in the absence of external magnetic field, therefore, it is called zero field splitting (ZFS). In this work ZFS will be expressed through extended Steven's operators:

$$\hat{H}_{ZFS} = \sum_{k} \sum_{-k \le q \le k} f b_k^q \hat{O}_k^q \tag{6}$$

where f – numeric constants; b_k^q – ZFS parameters, which are determined by the effective spin of the system and the paramagnetic centre symmetry. [2]

Interaction between the valence electrons and the nuclear magnetic moment results as additional hyperfine structure (HFS) of the EPR spectra. If the nucleus of an atom consists of an odd number of protons and/or neutrons it has a non-zero nuclear spin I value. In such case the unpaired electron spin is subjected not only to the external magnetic field, but also to local magnetic fields created by the nuclear spin magnetic moments, which leads to a splitting of lines into $2I+1$ components with equal intensities. The transitions are allowed between states where $\Delta M_s = 1$ and $\Delta M_I = 0$, and the separation between components is described by the hyperfine tensor $\tilde{A}$ [2]:

$$\hat{H}_{HFS} = \hat{S}\tilde{A}\hat{I} \tag{7}$$

2.1.3. EPR experiment

The realization of an EPR experiment is illustrated in fig. 2.2. The main components of an EPR spectrometer are a magnet system, resonator, microwave bridge, control and recording electronics.

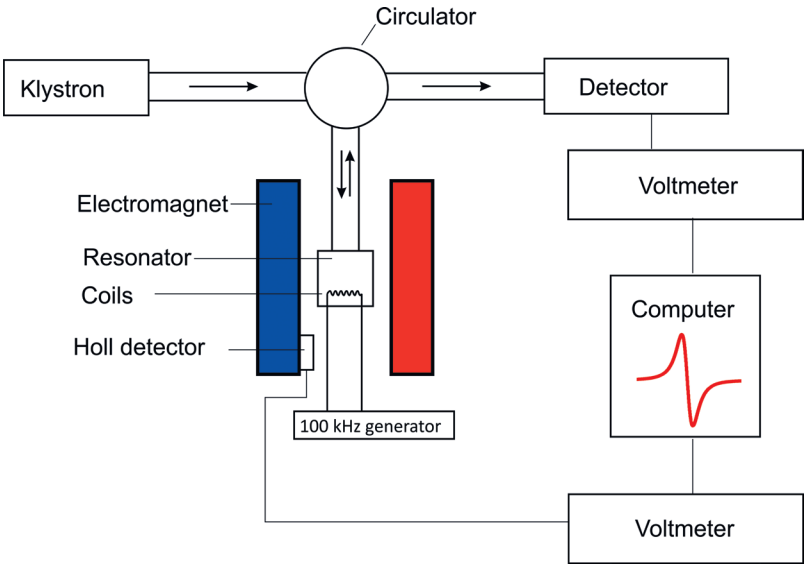

Fig. 2.2. **Realization scheme of an EPR experiment.**

The static magnetic field to ensure the splitting of the spin states is generated by an electromagnet system, which usually consists of two Helmholtz coils. In EPR experiments the magnetic field is increased linearly and when resonance condition (4) is met, transition between spin states is recorded. Important parameter of the magnet system is the achievable magnetic field range, which for X-band EPR spectrometers is usually 0 – 1 T (0 – 10000 G). The stability of magnetic field is ensured by power source, which regulates fluctuations in the field value using a Hall effect sensor. As the sensor cannot be positioned precisely in the sample location, additional calibration is necessary. Dyphenilpicrylhydrazyl (DPPH) with $g \approx 2.0036$ is one of the most commonly used reference samples for calibration purposes. To improve the signal-to-noise ratio the static magnetic field is modulated with 100 kHz frequency. A side effect of modulation is the registration of microwave absorption in the form of first derivative. [3]

Between the poles of electromagnet a resonator is situated – a cylindrical or rectangular metal box, that accumulates microwave energy in the form of standing waves. The ratio of the accumulated energy and dissipated energy in

one cycle multiplied by 2π is called the *Q* factor. The magnetic field component of microwave radiation drives the transitions between the spin states, therefore, it should be maximal in the sample position. Consequently the electrical field component in the sample position is minimal and dielectric losses due to electric dipole transitions are reduced. [3,4]

For the generation of X-band electromagnetic radiation klystrons are usually used – special types of vacuum tubes where microwaves are amplified by moving electron beams. At the moment of resonance, microwaves are reflected from the resonator and a signal appears on the detector (the signal, which goes through the sample is compared to the original signal from the source). In continuous wave (CW) EPR spectroscopy the sample is continuously irradiated with microwaves. As a consequence of resonator construction and practical aspects, the microwave frequency is not altered during EPR measurements. [3]

2.1.4. EPR spectra simulations

Numeric simulations essential for magnetic resonance spectra analysis nowadays can be done on practically any personal computer. Several computer programs (EasySpin [5], Visual-EPR [6], Xsophe [7] etc.) have been created that allow EPR spectra calculations and comparison with experimental results. An important peculiarity of EPR spectroscopy is the availability of SH parameters in scientific literature and databases, which allows efficient comparison of experimental results (resonance positions and intensities) with paramagnetic centres observed before.

For successful EPR spectra simulations it is necessary to choose a suitable model. Usually paramagnetic systems are described by a SH, which depends only on electron and nuclear spins while the effects of crystalline field and spin-orbital interactions are "hidden" is SH parameters.

In the beginning of EPR spectra simulations, first, the number and type of electron and nuclei spins must be chosen. In many cases, the choice of system's effective spin is obvious – for example, for organic radicals $S = 1/2$, whereas in transition metal and rare earth ions all unpaired outer shell electrons can be described with one effective spin value – in the case of Gd^{3+}, for example, $S = 7/2$. The choice of system's spin is more complex in cases when paramagnetic centres interact with each other creating composite systems and clusters. The choice of interacting nuclei in many cases is also simple – for example, in EPR simulations of copper complexes, HFS interaction with a Cu nuclear spin should be considered. Sometimes interactions with other neighbouring nuclei are resolved as the superhyperfine structure (SHFS) of the EPR spectra. [8]

After the choice of the spin system, it is necessary to choose which SH terms to include in the model. Every effective spin *S* in the system must have an electron-Zeeman interaction term. If $S > 1/2$ an additional ZFS term must be included, which mainly describes the effect of the crystalline field on the studied

system. Every nuclear spin I and S pair must have a corresponding HFS term. Of course, nuclei themselves also feel Zeeman effect, however, it is usually not detected in EPR spectra and, therefore, included in the SH.

The calculation of energy levels for a given SH and magnetic field value can be done with either diagonalization or perturbation techniques. In the diagonalization method SH is expressed as an N x N matrix, where N is the number of spin state in the system. The method gives accurate results within the range of calculation error, however, the required computational resources scale as N^3, so it becomes impractical for large spin systems. An alternative for systems with a small ZFS or HFS compared to the Zeeman term is to use the perturbation theory. First, the energy levels are analytically calculated for the electron-Zeeman interaction and other interactions are added as a perturbation. The next step of EPR calculations is to determine the resonance fields, that is, the magnetic field values for which the energy of microwave photon $h\nu$ matches the energy difference between the states. [8]

For EPR spectra simulations in solids the distribution of paramagnetic centre orientations is important. The orientation of the paramagnetic centre in respect to laboratory reference frame is given through Euler angles – three consequent rotations by which one coordinate system can be changed in the other. Two limiting cases are distinguished – single crystals, where only discrete centre orientations are possible and polycrystals, where all orientations are with equal probability. The resonance condition (4) thus is:

$$h\nu = g(\theta,\phi)\mu_B B \tag{8}$$

where the spectroscopic splitting factor at every orientation has an effective value, which can be calculated through diagonal $\tilde{g}$ tensor elements:

$$g(\theta,\phi) = \sqrt{\sin^2\theta\cdot\cos^2\phi\cdot {g_{xx}}^2 + \sin^2\theta\cdot\sin^2\phi\cdot {g_{yy}}^2 + \cos^2\theta\cdot {g_{zz}}^2} \tag{9}$$

θ and ϕ are the polar angles between the magnetic field and $\tilde{g}$ tensor Z axis. For a correct single crystal spectra calculation it is necessary to describe the orientation of SH tensor in the paramagnetic centre, the orientation of the paramagnetic centre within the crystal and the orientation of crystal axis in respect to laboratory reference frame. [8]

In samples where centres are chaotically oriented a (θ,ϕ) grid must be chosen where at every point a single crystal EPR spectrum will be calculated. Afterwards all spectra from the grid are combined to obtain the resulting powder spectrum. The smoothness of the calculations depends on the chosen grid.

The disorder in solids which is found in glasses and other amorphous media can be simulated by taking a distribution of SH values instead of discreet values. In a simple case it could a Gauss distribution function and as a result lines in the calculations would be broadened. [8]

The dream of every EPR practitioner is, of course, a simulation software, which could automatically parameterize a given EPR spectrum, however, in reality such spectrum fitting is possible only in cases where the initial model (the spin system, SH interactions and parameter values) already produce a result which is close to the experimental data.

2.2. S-state ions

Ions with half-filled outer electron shell are called S-state ions (resulting orbital moment $L = 0$, therefore, the ground state is the S state). Usually the following configurations are distinguished:

- $[Ar]^3d_5$; ground state – $^6S_{5/2}$ (Mn^{2+}, Fe^{3+})
- $[Xe]^4f_7$; ground state – $^8S_{7/2}$ (Eu^{2+}, Gd^{3+}) [9]

The outer shell's orbitals are filled according to empirical Hund's rules and the Pauli principle. $4f^7$ (Eu^{2+}, Gd^{3+}) electron configuration creates $^8S_{7/2}$ ground state – so, $S = 7/2$, $L = 0$ and $J = 7/2$. In this thesis the structure of Gd^{3+} and Eu^{2+} ions is studied in solids, therefore figure 2.3 shows the splitting of $^8S_{7/2}$ ground state in magnetic field presence. [2]

For a free ion the ground state is not split. As S-state incorporates into a solid, the crystalline field removes degenerancy from energy levels with different absolute spin projection values. This splitting occurs in the absence of external magnetic field and is called zero field splitting (ZFS). When magnetic field is applied, each spin projection acquires additional energy through Zeeman effect according to the equation (2). In the low field region the energy dependence on magnetic field value in nonlinear. A microwave radiation quantum with energy hv can excite transitions where $\Delta M_S = 1$. The expected EPR spectrum, therefore, consists of 7 resonances. [9]

Sometimes HFS can be resolved in the EPR spectra of Gd^{3+} and Eu^{2+}. For gadolinium only ^{155}Gd and ^{157}Gd isotopes with combined natural abundance of 31% are magnetic. It means that less that 1/3 Gd^{3+} centres are subjected to the HFS interaction. The nuclear spin $I = 3/2$ splits each Zeeman line into 4 components, however, the magnetic moments of isotopes are so small, that only in rare cases the linewidth of EPR lines allows to resolve this structure.

The nuclei of europium ions possess a more significant nuclear magnetic moment. ^{151}Eu and ^{153}Eu isotopes with $I = 5/2$ have a total of 100 % natural abundance, therefore, for all Eu^{2+} paramagnetic centres HFS interaction is present. The ratio of magnetic moments determines that there will be two types of Eu^{2+} centres for which the magnitude of HFS splitting will differ approximately 3 times. In such case, a 2 signal superposition must be used for EPR spectra simulations. In single crystals the HFS structure of europium centres is typically well resolved, however, in polycrystalline samples the averaging of all orientations may lead to a significant broadening of the observed spectrum.

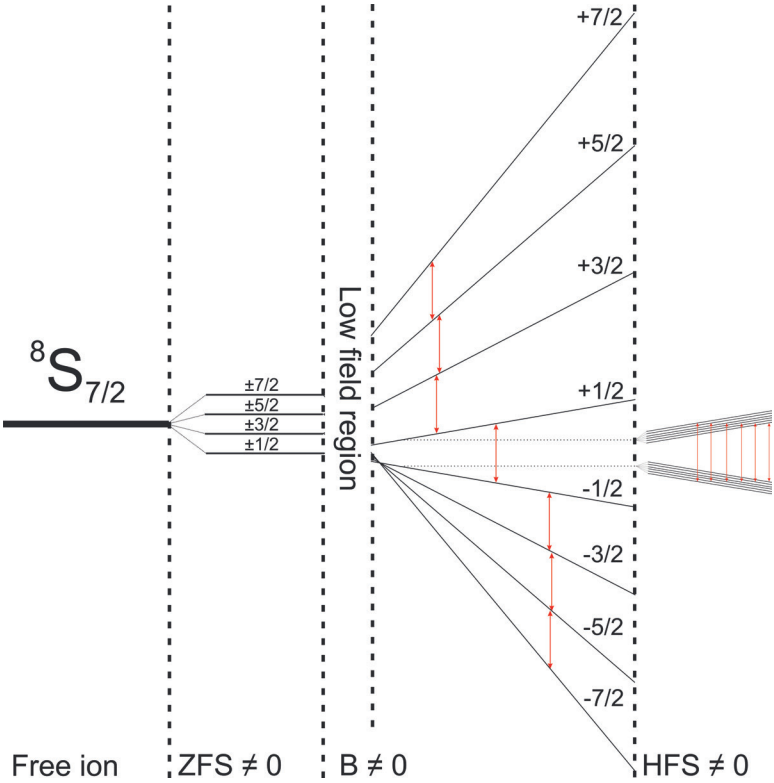

Fig. 2.3. **Splitting of $^8S_{7/2}$ ground state in external magnetic field.**

3. METHODOLOGY

3.1. The studied samples

The undoped ScF_3 single crystalline sample was synthesized in Russia (V. N. Voronov, L. Kirensky Institute of Physics, Krasnoyarsk). The sample orientation was done in EPR spectrometer from Gd^{3+} spectra angular dependences. From the experiments it was determined that one of the crystallographic axis is deviated from the sample holder axis by 13 °.

The undoped BaY_2F_8 single crystal was grown in Brazil (S. Baldochi, Nuclear and Energy Research Institute, University of Sao Paulo) by the zone melting method. The sample was oriented along its main crystallographic b axis by X-ray diffraction technique.

The impurities in the studied single crystals were analysed with X-ray fluorescence and optical spectroscopy methods.

In this work gadolinium and europium doped aluminosilicate oxyfluoride glasses and glass ceramics are also studied. For the preparation of glass samples a total of 8 g of high purity commercial ingredients were carefully weighed and mixed in ratios indicated in table 3.1. The ingredients were melted for 45 min at 1450 °C in Al_2O_3 crucibles using Carbolite HTF 18/8 furnace. Afterwards the melt was cooled rapidly by pouring it onto a stainless steel plate a pressing with another steel plate. In all cases transparent and colourless glasses were obtained. The samples were analysed with differential thermal analysis measurements, to determine the crystallization temperatures of different crystalline phases.

Table 3.1. **The initial powder compositions for glass preparations.**

Abbreviation	Ingredients (mol %)
C_Gd	$46SiO_2$-$20Al_2O_3$-$8CaCO_3$-$26CaF_2$-$0{,}1Gd_2O_3$
B_Gd	$40SiO_2$-$25Al_2O_3$-$15Na_2CO_3$-$20BaF_2$-$0{,}1GdF_3$
S_Gd	$40SiO_2$-$25Al_2O_3$-$15Na_2CO_3$-$20SrF_2$-$0{,}1GdF_3$
S1_Eu	$40SiO_2$-$25Al_2O_3$-$15Na_2CO_3$-$19SrF_2$-$1EuF_3$
S2_Eu	$50SiO_2$-$20Al_2O_3$-10NaF-$19SrF_2$-$1EuF_3$

The glass ceramics were obtained with the heat treatment method by heating the initial glass sample at a fixed temperature for 1 h. The names of samples in this work include the abbreviation of the composition as well as the thermal treatment temperature. For example, C_Gd_PG is the C_Gd composition precursor glass sample, but C_Gd_600 is the corresponding glass ceramic obtained by heating the C_Gd_PG sample at 600 °C for 1 h.

The crystalline phases in glass ceramics were determined by X-ray diffraction measurements. For sample visualization and crystallite size distribution estimation transmission electron microscopy measurements were made. The optical properties of glasses and glass ceramics were characterized by absorption, transmission and photoluminescence techniques. The EPR measurements were made at 77 K by inserting the sample in a dewar filled with liquid nitrogen and pressing it with a sample holder in order to avoid sample movement during the measurements.

3.2. Methods

EPR measurements were made with a modified RE 13-06 EPR spectrometer. The magnetic system ensured magnetic field range of 350–5800 G. The X-band microwave radiation was generated by klystron at $f \approx 9.1$ GHz. The accuracy of frequency was controlled with 0.001 GHz accuracy. The magnetic field value was calibrated with DPPH reference with $g = 2.004 \pm 0.001$. The measurements were carried out at room (≈ 295 K) and liquid nitrogen boiling (77 K) temperatures by inserting the sample in a dewar and submerging it in liquid nitrogen if necessary.

EPR spectra simulations were done in EasySpin [5] and Visual EPR [6] programs. Easyspin is a freeware based on Matlab environment which is exceptionally suited for magnetic resonance spectra simulations. Here it was employed to calculate the EPR spectra of chaotically oriented crystalline phases in glass ceramics. EPR spectra angular dependences in single crystals were parameterized using Visual EPR. For a correct defect model and SH choice the program varies the SH parameter values using the least square fitting methods to achieve the best agreement with experimental data.

Impurity elements in single crystalline samples were analysed using X-ray fluorescence (XRF) spectra measurements with EDAX/Ametek Eagle III microanalyzer. The fluorescence was excited with X-rays from a rhodium lamp focused through multicapillary lens with effective diameter 50 μm.

For the orienting of BaY_2F_8 single crystal and identification of crystalline phases in glass ceramics PANalytical X'Pert Pro diffractometer with copper anode (Cu Kα) operated at 45 kV and 40 mA was used. Crystalline phases were identified from Crystallography Open Database [10–12]. The visualization

of crystalline phases was done in VESTA software. [13,14] The crystallite size estimation was done by Rietvield spectral peak analysis.

The transmission electron microscopy (TEM) images for glass ceramics were obtained by Tecnai G2 F20 microscope operated at 20 kV voltage. Samples were prepared as described in [15,16].

Differential thermal analysis (DTA) measurements were made with Shimadzu DTG-60 thermogravimetric analyser. For DTA purposes the samples were grinded in homogenous powder and weighed in equal mass with reference powder Al_2O_3. The measurements were made with a 10 °C/min heating rate.

The absorption spectra of glass ceramics were recorded with Analytik Jena SPECORD-210 UV-VIS spectrophotometer.

In photoluminescence measurements Andor Technology spectrometer SR-303i-B with Andor CCD DU-401-BV was used. Hamamatsu xenon lamp C2577 and tunable impulse laser Ekspla NT342/3UV were used as excitation sources.

4. RESULTS

4.1.Scandium fluoride

Scandium trifluoride (ScF_3) is a cubic ABX_3 structure perovskite with A position vacant. Unlike many other metal fluorides MF_3, which have a rhomboedric structure at room temperature, this crystal has a cubic Pm-3m structure. [17–19] Figure 4.1 shows the cubic structure of ScF_3 – each Sc^{3+} ion is coordinated with six equidistant fluorine anions. At increased pressure a phase transition to R-3c phase occurs. Unlike other materials of this class, ScF_3 has a negative thermal expansion (NTE) coefficient, meaning that upon heating the material the lattice constant shrinks, not increases. [20] The NTE effect of the simple cubic structure is profound ever at room temperature, therefore, ScF_3 is a good model material, which has attracted a lot of scientific interest. [21–27]

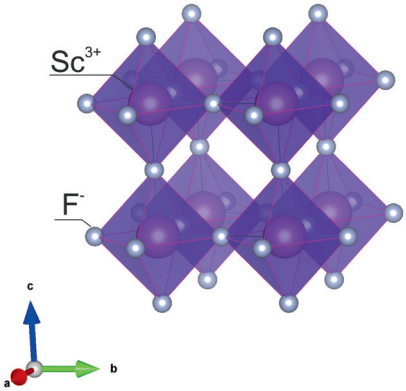

Fig. 4.1. **The cubic structure of ScF_3.**

In the case of S-state ion impurities (Mn^{2+}, Gd^{3+}) it has been observed that they substitute Sc^{3+} ions isomorphously conserving local cubic site symmetry. [28] In the case of Mn^{2+} (S = 5/2) EPR spectra consist of six sets of lines with g = 2.00138. For Gd^{3+} (S = 7/2) impurities in this host a characteristic ZFS structure is seen in the EPR spectra around g = 1.992 similar to other cubic fluoroperovskites [29–33]. In a later study [32] it was found that the SH parameter values for ScF_3:Gd^{3+} determined in [28] are inconsistent.

The XRF and photoluminescence analysis of the studied ScF_3 sample did not detect any impurities. In EPR measurements at 77 K a set of seven lines characteristic for Gd^{3+} was detected for which angular dependences were recorded at room temperature and 77 K. The resonance position maps are shown in figure 4.2. The EPR spectra were measured with a 5 ° increment in a range of 90 °. The 0 ° position spectrum was chosen as the position with maximum splitting in the magnetic field range. After a 90 ° rotation the observed spectrum is not as wide. From this fact in simulations a deviation of 13 ° for the rotation axis from crystallographic axis was calculated. Spectra exhibit a symmetry around 45 ° position indicating a cubic site symmetry for the impurity.

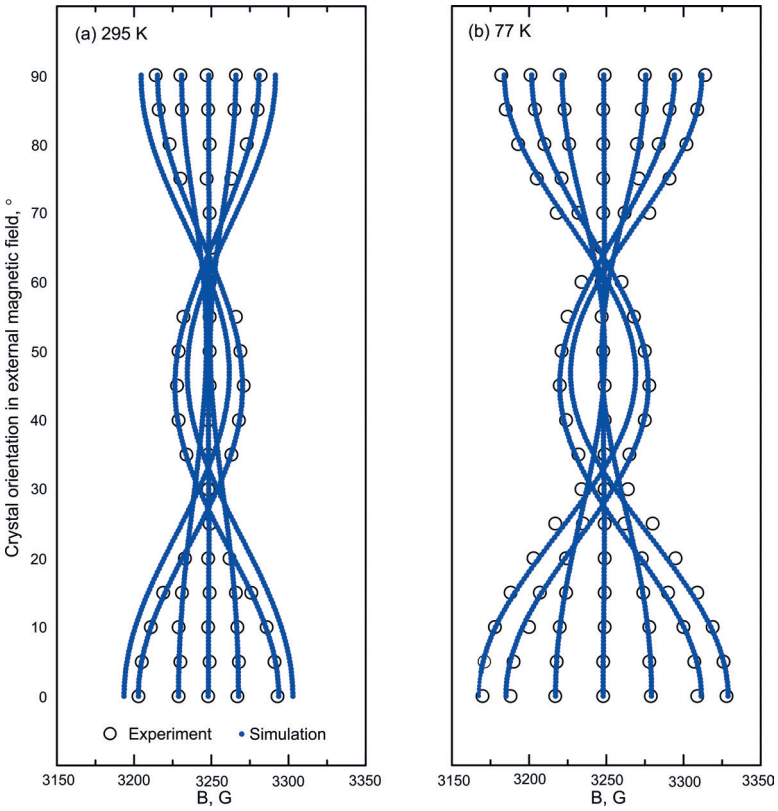

Fig. 4.2. **EPR spectra resonance maps and calculation lines in ScF_3 at (a) 295 K; (b) 77 K.**

In EPR spectra simulations an effective spin $S = 7/2$ system in cubic field symmetry was chosen. SH for cubic ZFS is:

$$\hat{H} = \hat{H}_{EZ} + \hat{H}_{ZFS} = g\mu_B \hat{S}\vec{B} + \frac{b_4}{60}\left(\hat{O}_4^0 + 5\hat{O}_4^4\right) + \frac{b_6}{1260}\left(\hat{O}_6^0 - 21\hat{O}_6^4\right) \qquad (10)$$

The variable parameters in simulations are the spectroscopic splitting factor g and the cubic fourth and sixth order ZFS parameters b_4 and b_6. The calculated parameter values are $g = 1.992 \pm 0.001$ and:

- $b_4 = (-2.73 \pm 0.02)\cdot 10^{-4}$ cm^{-1} and $b_6 = (0.67 \pm 0.01)\cdot 10^{-4}$ cm^{-1} (295 K);
- $b_4 = (-3.96 \pm 0{,}02)\cdot 10^{-4}$ cm^{-1} and $b_6 = (0.78 \pm 0{,}01)\cdot 10^{-4}$ cm^{-1} (77 K).

The average deviation between experimental resonances and simulations lines are 1.2 G at 295 K and 2.5 G at 77 K. The signs of ZFS parameters are taken from studies of similar materials.

ZFS parameter $|b_4|$ in ScF_3 at 295 K and 77 K shows a similar behaviour as fluorides, which expand positively with temperature. A clear demonstration of this is shown in figure 4.2 – the $|b_4|$ values are linearly dependent on temperature and despite the NTE coefficient of ScF_3, the temperature behaviour is similar. Therefore, crystal thermal expansion effects alone cannot explain the observed temperature dependence of ZFS parameters.

For a more quantitative estimation a thermodynamic model from [33] was used:

$$\left(\frac{\partial b_4}{\partial T}\right)_V = \left(\frac{\partial b_4}{\partial T}\right)_p - \left(\frac{\beta}{K}\right)\left(\frac{\partial b_4}{\partial p}\right)_T \qquad (11)$$

where β and K ir are the volume thermal expansion and compressibilty coefficients respectively. The assumption made in [33] that the ratio of β/K around the paramagnetic centre is similar as in the bulk crystal is not valid for ScF_3, because the NTE value of β would produce a different slope coefficient for the temperature dependence (visible as the calculation line in fig. 4.3).

In order to achieve the experimental b_4(T) dependence for ScF_3 with model (11), a positive β value is necessary. Due to perpendicular oscillations $\Delta u_\perp$ of atoms perpendicularly to bonds the average distance between ligands R_v is always larger than the lattice constant R determined from XRD:

$$R_v = R + \frac{\left\langle \Delta u_\perp^2 \right\rangle}{2R} \qquad (12)$$

Extended x-ray absorption fine structure (EXAFS) measurements have shown that in crystals with NTE coefficient the average distance between atoms R_v always expands positively with temperature. [34] Studies have shown that the distances in the first coordination sphere in ScF_3 also expand positively with temperature. [24]

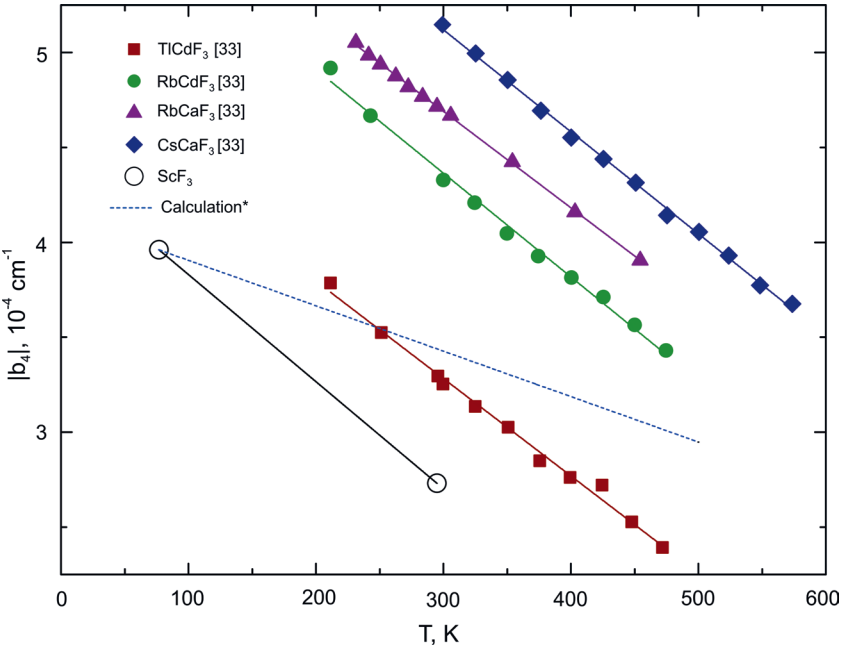

Fig. 4.3. **Temperature dependence of Gd^{3+} parameter $|b_4|$ in ScF_3 and other cubic fluorides.** [33] ***Calculation with the model (11) assuming the bulk β and K values in ScF_3.**

To summarize, the ZFS parameters determined here correlate with the average distances between atoms determined from EXAFS measurements. An important and fundamental conclusion that follows is that the interpretation of EPR spectra in crystals should be based on the real interatomic distances not just the crystallographic data determined from XRD measurements.

4.2. Barium yttrium fluoride

Barium yttrium fluoride (BaY_2F_8) is a monoclinic C2/m space group symmetry structure crystal (see fig. 4.4). The lattice constants are a = 6.972 Å; b = 10.505 Å; c = 4.260 Å; $\alpha = \beta = 90$ ° and $\gamma = 99.45$ °. b is the crystal's main symmetry axis, which forms a 90 ° angle with plane ac. Every Y^{3+} ion is coordinated with 8 F^- ions. [35] Due to a number of properties – transparency in a wide electromagnetic spectrum range, low phonon energy and good mechanical properties – BaY_2F_8 is a promising host for rare earth activators. [36–42]

The XRF analysis of the undoped BaY_2F_8 single crystal sample did not detect any additional impurities. The photoluminescence measurements revealed the presence of Dy^{3+}, Pr^{3+} and Er^{3+} ions in the sample. During EPR

measurements at room temperature several lines in a wide spectrum range were detected. The single crystal was oriented along its main symmetry axis b with XRD method and angular dependences were recorded at room temperature and 77 K. The resonance position map at 77 K together with simulation lines is shown in figure 4.5.

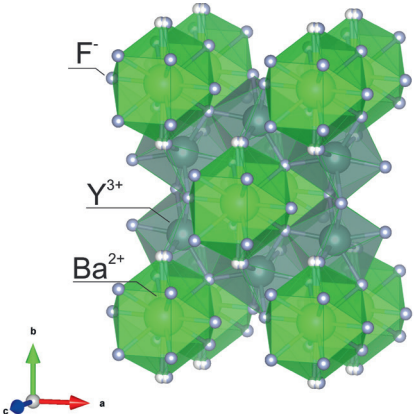

Fig. 4.4. **BaY_2F_8 structure.**

The observed angular dependence of the resonance lines in the wide spectrum range indicate a high S system in a low symmetry crystalline field. These results are similar to a monoclinic ThS_2:Gd^{3+} centre [43], therefore, in spectra simulations a $S = 7/2$ system was taken. In low symmetry crystals the axis of paramagnetic centre's coordinate system often do not coincide with crystallographic axis. Here the variable SH ZFS parameters were not fixed with symmetry constraints and the SH used in simulations was:

$$\hat{H} = g\mu_B \hat{S}\vec{B} + \sum_k \sum_q f_k b_k^q \hat{O}_k^q \qquad (13)$$

In some orientations of fig. 4.5 the simulated transitions lines do not exceed threshold probability values and are, therefore, not shown here. In the EPR experiment the corresponding lines were not detected due the low signal intensity of these transitions.

The obtained results indicate that a low symmetry Gd^{3+} centre has been observed in BaY_2F_8 crystal. It has been estimated that $g = 1.99$ and ZFS parameters $|b_2^0| > 850 \cdot 10^{-4}$ cm^{-1}; $|b_2^2| > 400 \cdot 10^{-4}$ cm^{-1}; $|b_2^1| > 300 \cdot 10^{-4}$ cm^{-1} and $|b_4^3| > 200 \cdot 10^{-4}$ cm^{-1}, however, for a precise determination of SH parameters additional measurements should be performed in additional orientations and full magnetic field range.

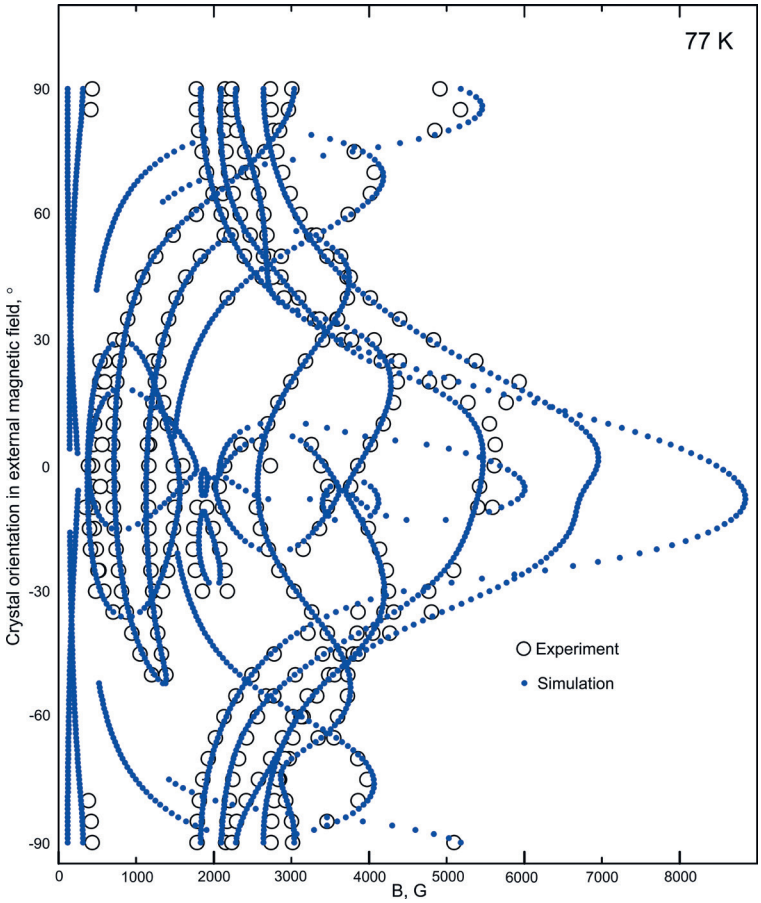

Fig. 4.5. **The angular dependence of resonance positions in BaY_2F_8 at 77 K.**

4.3. Gadolinium doped glass ceramics

Glass ceramics is a composite material with promising optical properties. It consists of a glass matrix, which contains nanosized particles of one or several crystalline phases. Figure 4.6 illustrates a glass and glass ceramic sample. Glasses are usually obtained by the conventional melt quenching technique. After the thermal treatment of the precursor glass, formation of crystalline phases occurs. By adjusting the glass composition and thermal heating procedure it is possible to control crystalline phases and their size in glass ceramics. [44,45]

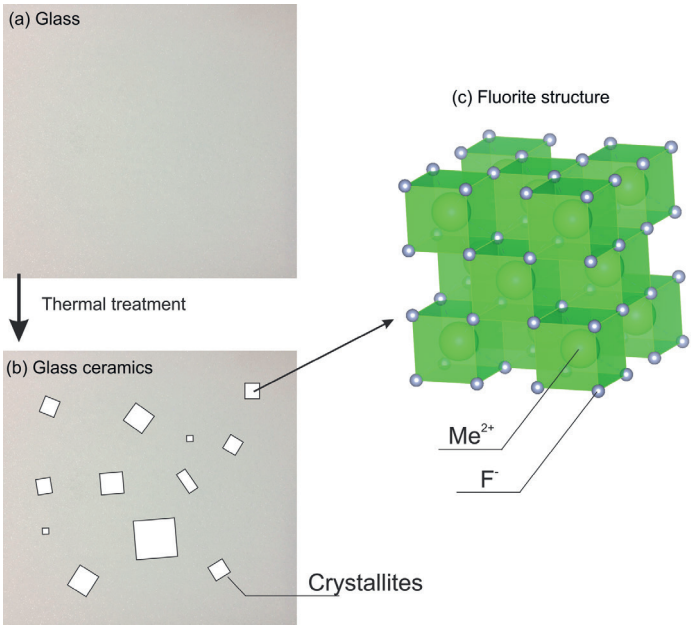

Fig. 4.6. **Illustration of a (a) glass; (b) glass ceramic and (c) fluorite structure crystal.** [44]

To detect the change of local structure around activators with EPR spectroscopy, the glass matrix can be doped with paramagnetic impurities. Although crystalline materials and glasses have been studied thoroughly by EPR, information in literature about the incorporation of activators in the crystalline phase of glass ceramics is somewhat scarce. A majority of glass-ceramic potential applications a related to rare earth ion luminescence, therefore, studies of trivalent ions in these systems are of great interest. EPR studies of rare earth ions are problematic – not all ions are paramagnetic (in principle cannot be studied with EPR) and spin-relaxation times are so short that liquid helium temperatures are necessary to resolve the spectra. Gadolinium is the only trivalent rare earth ion, for which EPR spectra can be detected at room temperature.

The incorporation of Gd^{3+} into the fluorite structure crystalline phases (CaF_2, BaF_2, SrF_2) is studied on C_Gd ($46SiO_2$-$20Al_2O_3$-$8CaCO_3$-$26CaF_2$-$0{,}1Gd_2O_3$), B_Gd ($40SiO_2$-$25Al_2O_3$-$15Na_2CO_3$-$20BaF_2$-$0{,}1GdF_3$) and S_Gd ($40SiO_2$-$25Al_2O_3$-$15Na_2CO_3$-$20SrF_2$-$0{,}1GdF_3$) compositions. The initial glasses where colourless and visually transparent. The samples were thermally treated at selected temperatures and systematically characterized with XRD and EPR methods. For some samples TEM images were taken. A summary of the results is given in figure 4.7 – on the left side the XRD measurements and on the right – the EPR spectra of the corresponding samples. The measurements are grouped

by compositions – from top to bottom – C_Gd, B_Gd and S_Gd. Each sample has 3 experimental measurements – the upper is the initial glass sample (_PG) and the remaining – glass ceramics obtained at indicated temperatures (the last number in the sample abbreviation). For XRD measurements the final curve is the calculated diffractogram for the polycrystalline fluorite phase by taking the data from [10–12] database. The average crystallite size for the primary crystalline phase is summarized in table 4.1.

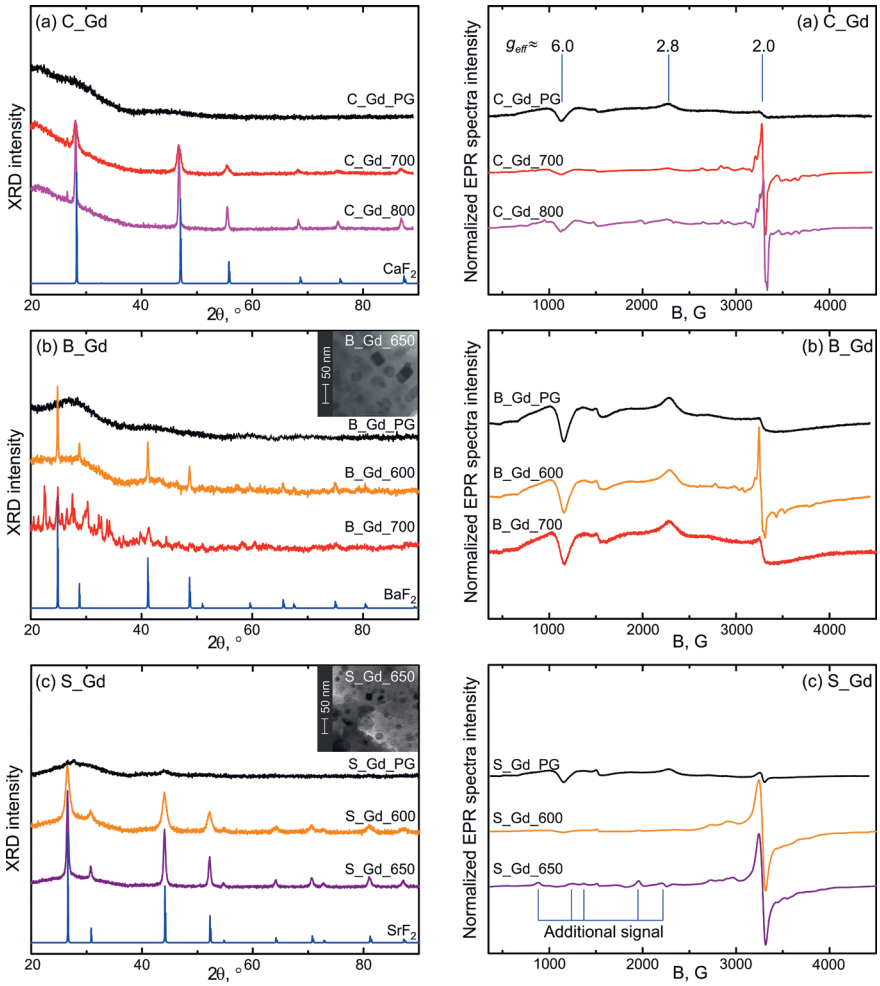

Fig. 4.7. **XRD and EPR spectra of (a) C_Gd, (b) B_Gd and (c) S_Gd oxyfluoride compositions with Gd^{3+} activators. For selected samples TEM images are included.**

In all studied compositions a range of temperatures exists where only the fluorite phase crystallizes and other crystalline phases are absent. In this case, the glassy Gd^{3+} EPR signal [46–53] is overlaid with intense fine structure centred around $g_{eff} \approx 1.99$. As this new signal correlates with the formation of CaF_2, BaF_2 or SrF_2 crystalline phases in glass ceramics it would be beneficial to understand the nature of various possible Gd^{3+} centres in the respective single crystals. If Gd^{3+} replaces a divalent cation in a MeF_2 structure crystal, a charge compensation is necessary. If the compensator is located beyond the first coordination spheres of Gd^{3+}, the site symmetry remains cubic. [54] It is possible, however, that a charge compensator in the vicinity (usually a F^- ion) lowers the local symmetry around the centre. [55–58] A reasonable first step for the interpretation of the fine structure in glass ceramics would, therefore, be simulations of the experimental EPR spectra with SH parameter values determined in the respective single crystals.

Table 4.1. **Estimation of the fluorite structure crystallite size (in nm) in glass ceramics from the XRD data.**

Sample	C_Gd	B_Gd	S_Gd
600		69 ± 3	10 ± 1
650	7 ± 1	52 ± 5	28 ± 1
700	14 ± 1		84 ± 15
800	51 ± 3		106 ± 30

In spectra simulations the following SH were used [9]:

- for cubic symmetry:

$$\hat{H} = g\mu_B \hat{S}\vec{B} + \frac{b_4}{60}\left(\hat{O}_4^0 + 5\hat{O}_4^4\right) \tag{14}$$

- for tetragonal symmetry:

$$\hat{H} = g\mu_B \hat{S}\vec{B} + \frac{1}{3}b_2^0\hat{O}_2^0 + \frac{1}{60}\left(b_4^0\hat{O}_4^0 + b_4^4\hat{O}_4^4\right) \tag{15}$$

- for trigonal symmetry:

$$\hat{H} = g\mu_B \hat{S}\vec{B} + \frac{1}{3}b_2^0\hat{O}_2^0 + \frac{1}{60}\left(b_4^0\hat{O}_4^0 + b_4^3\hat{O}_4^3\right) \tag{16}$$

The uncertainty of SH parameters in glass ceramics is much higher than found in literature [54–58] as could be expected from averaging all possible orientations in chaotically oriented systems. Nevertheless, the SH parameter values obtained here within the error limits correspond well with studies of

single crystals, and the spectral simulations with these values (in fig. 4.8) reproduce the experimental spectra with high precision. The conclusion to be drawn is that in oxyfluoride glass ceramics with fluorite crystallites the EPR spectra fine structure arises from isolated Gd^{3+} centres which have been previously identified in single crystals.

It is interesting to note, that in some glass ceramics only cubic Gd^{3+} are present, but, for example, in samples containing BaF_2 – only Gd^{3+} in trigonal site symmetry is detected, although cubic centres have been observed in CaF_2 and SrF_2 as well as BaF_2 single crystals. The ionic radii of Gd^{3+} and Ca^{2+} are similarly sized and the glass ceramics with CaF_2 have only cubic Gd^{3+} centres. The mismatch of Gd^{3+} and Ba^{2+} radii, on the other hand, is significant and only lower symmetry centres are observed. It is intuitive to assume that if an impurity substitutes another ion in the lattice the size mismatch can lead to a considerable distortion and as a result – a lowering of local symmetry. For similarly sized ions the impact on the crystalline field could be expected small enough to leave the initial site symmetry intact. Such simplistic model correlates well with the observed Gd^{3+} EPR spectra in glass ceramics.

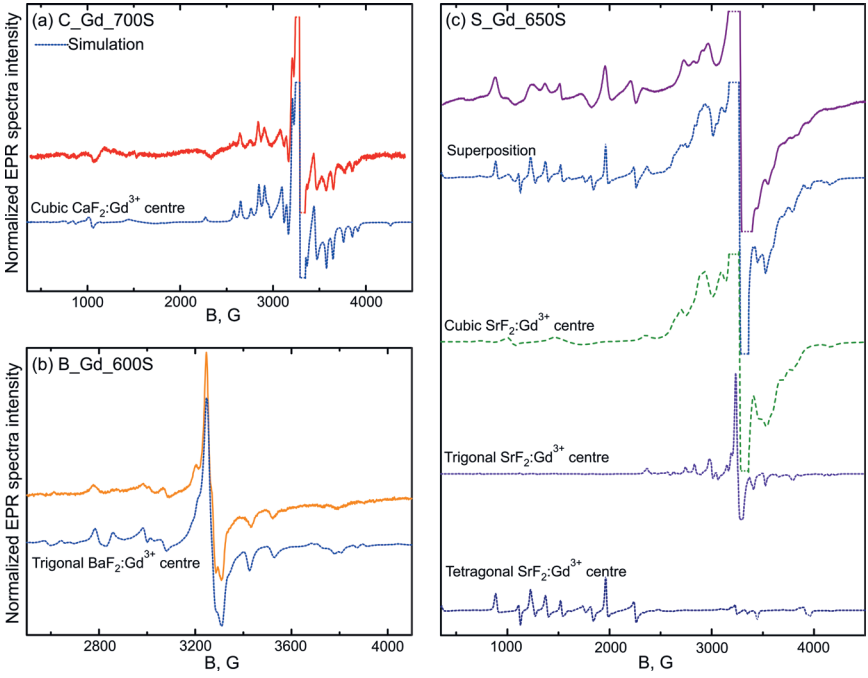

Fig. 4.8. **EPR spectra simulations of glass ceramics containing (a) CaF_2, (b) BaF_2 and (c) SrF_2 crystalline phases.**

4.4. Europium doped glass ceramics

Glass ceramics are actively studied as a host material for white light emitting diodes (WLEDs). [59–65] In the current commercial realization the white light is achieved by a combination of a blue (InGaN 450-470 nm diode) excitation source and a green or red phosphor. The widely used Ce:YAG ($Y_3Al_5O_{12}$:Ce^{3+}) phosphor is thermally unstable which leads to a loss of efficiency at higher operational temperatures. [65] The high thermal, chemical and mechanic stability of glass ceramics makes them a promising alternative. [66] Europium is one of the commonly used rare earth activators in the development of optically active materials. There are two stable valence states, where the optical properties are governed by either *4f-4f* (Eu^{3+}) or *5d-4f* (Eu^{2+}) transitions. In order to develop a suitable glass ceramic knowledge about the influence of composition on the valence state of europium and its local structure is necessary.

The properties of europium ions are studied in ($40SiO_2$-$25Al_2O_3$-$15Na_2CO_3$-$19SrF_2$-$1EuF_3$) and S2_Eu ($50SiO_2$-$20Al_2O_3$-10NaF-$19SrF_2$-$1EuF_3$) oxyfluoride compositions. The S2 contains more fluorides, therefore, increased sample self-crystallization is expected. The XRD and EPR measurements are summarized in figure 4.9. Both compositions exhibit self-crystallization and in the S2 composition the initial average size of SrF_2 crystallites exceeds 10 nm. After heat treatment at 650 °C both samples contain similarly sized SrF_2 crystallites (the size estimations from the XRD data are summarized in table 4.2). Typical TEM images confirm a rather good homogeneity of crystallite size distribution and also indicate that crystallization upon heating is more pronounced in composition S1. After thermal treatment above 700 °C secondary crystalline phases are detected – in the S1_Eu_800 sample the additional XRD peaks have a good match with nepheline ($NaAlSiO_4$) diffractogram. In the S2 composition formation of strontium feldspar crystallites at 800 °C suppresses the primary SrF_2 phase.

Table 4.2. **SrF_2 crystallite size estimation in nm in glass ceramics.**

Sample	S1_Eu	S2_Eu
PG		10 ± 1
600	7 ± 1	15 ± 1
650	21 ± 1	23 ± 2
700	60 ± 4	
800	117 ± 18	

EPR spectra of all samples show a resonance line at $g_{eff} \approx 4.3$, which is usually attributed to the presence of Fe^{3+} impurities in the glass. [67] The S1_Eu_PG does not contain any additional signals indicating that europium is in the 3+ (non-paramagnetic) valence state. In the thermally treated S1_Eu samples an additional signal at $g_{eff} \approx 2$ emerges with a distinct structure at 800 °C. This could be a consequence of $Eu^{3+} \rightarrow Eu^{2+}$ reduction after heat treatment at high temperatures. In the previous section, the EPR spectra of gadolinium doped glass ceramics were related to Gd^{3+} centres previously reported in the corresponding CaF_2, BaF_2 or SrF_2 single crystals, so it would be reasonable to attribute the additional structure of the S1_Eu_650 sample here with Eu^{2+} centres in SrF_2 phase. For this purpose a polycrystalline SrF_2:Eu2+ was synthesized. The EPR spectra of SrF_2:Eu^{2+} and S1_Eu_650 are compared in figure 4.10. The simulation curve shows the cubic SrF_2:Eu^{2+} signal. [68] The remaining resonances are simulated in figure 4.11 by parameter values in table 4.3 and the following SH:

$$\hat{H} = g\mu_B \hat{S}\vec{B} + \frac{1}{3} b_2^0 \hat{O}_2^0 + A_i \hat{S}\hat{I} \qquad (17)$$

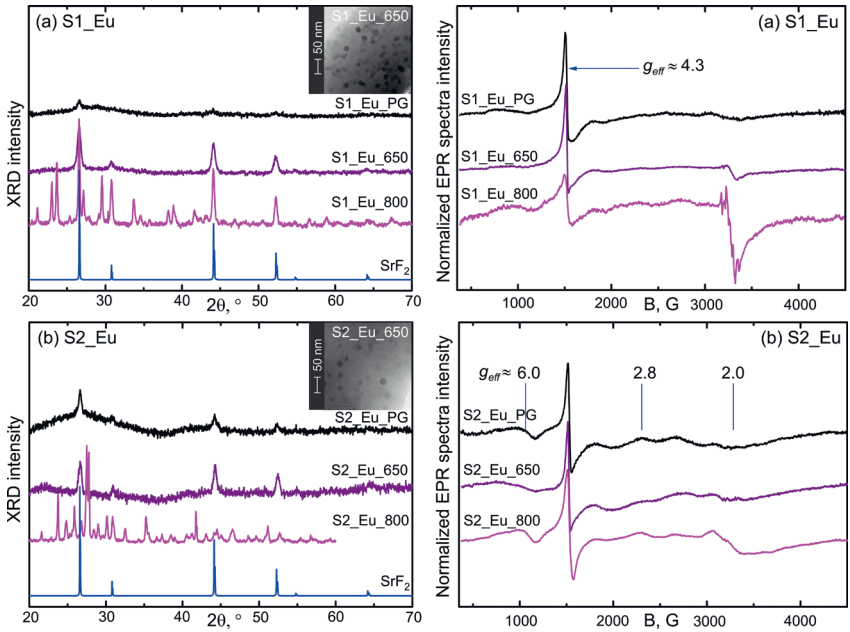

Fig. 4.9. **The XRD un EPR spectra of (a) S1_Eu and (b) S2_Eu oxyfluoride composition with europium activators. For the samples heated at 650 °C TEM images are shown.**

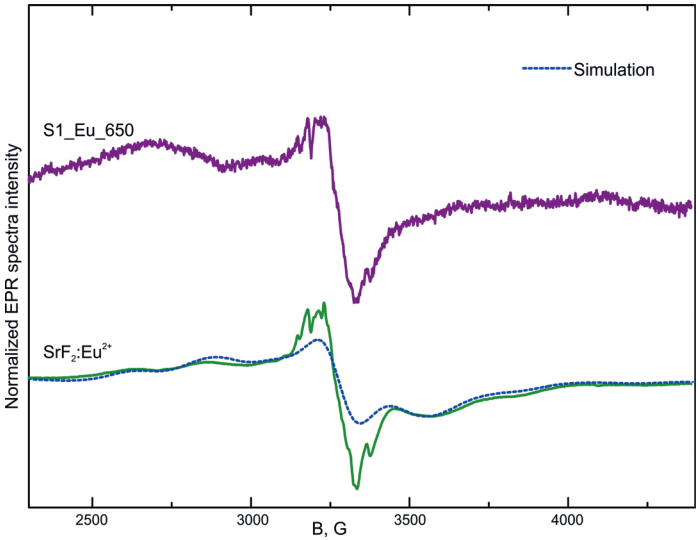

Fig. 4.10. **Comparison of S1_Eu_650 glass ceramic and polycrystalline $SrF_2:Eu^{2+}$ EPR signals. Simulation with cubic SH and parameters from [68].**

Table 4.3. **The determined SH (17) parameter values in the simulations of signals shown in fig. 4.11.**

Sample	S1_Eu_650	S1_Eu_800
g	1,978 ± 0,002	1,992 ± 0,002
b_2^0, 10^{-4} cm^{-1}	15 ± 5	10 ± 5
A_{151Eu}, 10^{-4} cm^{-1}	- 34 ± 1	- 33 ± 1
A_{153Eu}, 10^{-4} cm^{-1}	- 15 ± 1	- 15 ± 1

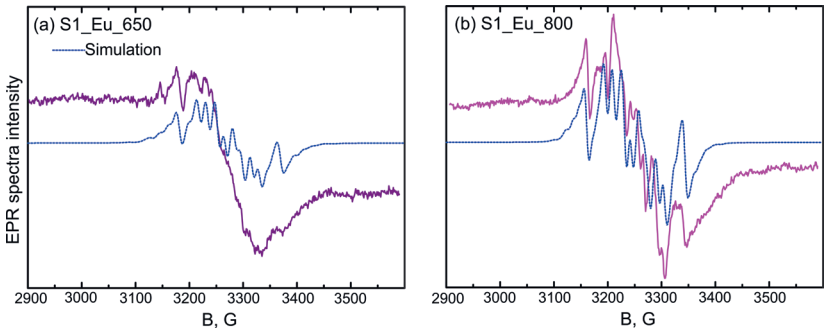

Fig. 4.11. **Simulations of (a) S1_Eu_650 and (b) S1_Eu_800 EPR spectra with SH (17) and parameters from table 4.3.**

In the S2_Eu composition intitial sample EPR spectrum wide envelope curves are observed with singularities at g_{eff} = 6.0, 2.8 and 2.0 – that is, the so called S = 7/2 S-state ion spectrum in the disordered environment (U-type spectrum), which means that the S2 composition is not only self-crystallized, but also self-reduced. Although the S2_Eu_PG already contains crystallites with average size around 10 nm, the EPR signal comes from Eu^{2+} ions in the glassy phase. It is possible that in the initial glass matrix Eu^{2+} is coordinated mainly by oxygen and bonds with fluorine anions during thermal treatment are not formed. The decreased overall crystallinity compared to S1_Eu_650 as visible in the TEM images in figure 4.9 could also contribute to the lack of SrF_2:Eu^{2+} signal in the S2_Eu_650 sample.

Photoluminescence measurements after laser excitation with 350 nm are shown in figure 4.12. This wavelength excites Eu^{2+} luminescence and as a result the spectra consist of wide bands. A significant impact of the chosen composition and the heating temperature can be seen. The S1_Eu_PG sample contains barely any Eu^{2+}, however, the intense blue band in the S2_Eu_PG sample confirms the composition's abundance with divalent europium. This correlates with the EPR measurements shown in figure 4.9, which detected Eu^{2+} ions in the disordered phase in the S2 composition samples. Some reduction after thermal treatment at 650 °C is visible in the S1, however luminescence is still an order of magnitude weaker than in S2. Efficient $Eu^{3+} \rightarrow Eu^{2+}$ reduction occurs occurs only after heating the samples at 800 °C, which is accompanied by the formation of complex silicate structures in the samples. Based on the XRD and EPR data, as well as literature analysis the origin of luminescence bands could be explained as:

- S1_Eu_800 550 nm – $NaAlSiO_4$:Eu^{2+} centres [69,70];
- S1_Eu_800 390 nm – Eu^{2+} ions in sodalite-like structure;
- S2_Eu_PG un S2_Eu_650 420 nm– Eu^{2+} ions in the glassy phase of glass ceramics;
- S2_Eu_800 406 nm – Eu^{2+} ions in strontium feldspar phase [71,72].

As visible from the EPR as well as photoluminescence spectra the efficiency of europium reduction in oxyfluoride glass ceramics increases significantly with high sample treatment temperatures. Such behaviour has previously been reported and explained in geological samples. [73]

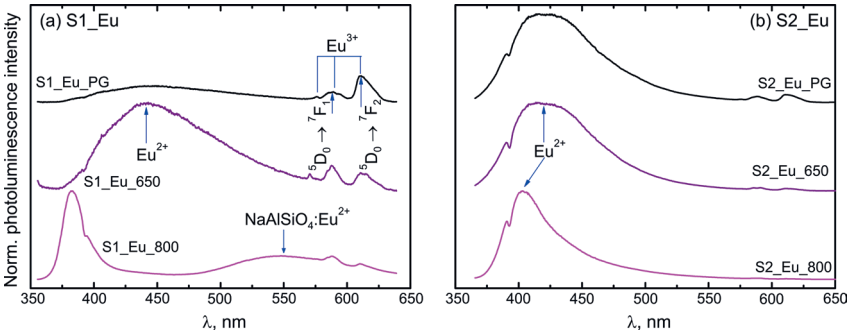

Fig. 4.12. **Photoluminescence of (a) S1_Eu and (b) S2_Eu samples after 350 nm excitation.**

The differences in the optical properties of S1 and S2 samples are, of course, determined by the chemical composition. The S2_Eu contains more fluorine ions, which stimulates the phase separation and self-crystallization of the sample. Previous studies have reported improved $Eu^{3+} \rightarrow Eu^{2+}$ conversion upon increasing the fluorine content in the composition. [74] In glasses the reduction of europium is mainly determined by the electronegativity of the local structure. For quantitative calculations the optical basicity model is often employed in which electron density on oxygen must be estimated. Below a critical optical basicity value, europium in the 2+ valence state in the glass network is favoured over 3+. [74,75] The increased fluorine content of the S2 composition increases the self-crystallizatin effect upon casting and decreases the optical basicity of the sample stimulating the $Eu^{3+} \rightarrow Eu^{2+}$ reduction. Although the S2_Eu_PG already contains SrF_2 crystallites, the EPR signal and the corresponding blue luminescence originates from Eu^{2+} ions in the amorphous phase.

In glass ceramics the $Eu^{3+} \rightarrow Eu^{2+}$ phenomenon is also sometimes explained through the charge compensation model, where the reduction of europium when substituting a divalent cation in the lattice is required to preserve the charge neutrality. [76] As seen here, the heating temperature must be comparatively high for the reduction to be efficient.

CONCLUSIONS

The EPR spectra fine structure of S-state ions (Gd^{3+} and Eu^{2+}) has yielded valuable information about activator local structure in various materials. EPR spectra angular dependences of Gd^{3+} in fluoride single crystals as well as additional signals of S-state ions in the crystalline phases of glass ceramics have been studied thoroughly.

In ScF_3 – crystal with negative thermal expansion coefficient – EPR spectra parameters have been determined at two temperatures. The temperature dependence of the parameter values correlates with other cubic fluorides, which expand positively with temperature. It means, that the EPR spectra depend on the activator local structure, which differs from the bulk thermal expansion of the crystal.

A low symmetry Gd^{3+} centre has been observed in monoclinic BaY_2F_8 crystal. All experimentally detected resonances can be described by one set of spin-Hamiltonian parameters, which indicates that for trivalent impurities in small concentrations there is only one position in the crystal structure.

Gadolinium is a suitable paramagnetic probe to monitor the incorporation of activators in the crystalline phase of glass ceramics – the glassy U-type EPR spectrum is overlaid with intense fine structure characteristic to Gd^{3+} in the corresponding polycrystal. When a trivalent ions substitutes a divalent cation in glass ceramics with MeF_2 crystallites (Me = Ca, Ba, Sr), a charge compensator induced local symmetry reduction is expected. In cases when gadolinium replaces similarly sized Ca^{2+} and Sr^{2+} ions cubic Gd^{3+} centres are present in oxyfluoride glass ceramics. When the ionic radii differ significantly as for Gd^{3+} and Ba^{2+}, lower symmetry Gd^{3+} centres are observed.

In europium doped oxyfluoride compositions EPR spectroscopy allows to monitor the valence state of ions – Eu^{3+} does not produce any EPR signal, but the Eu^{2+} S-state configuration spectra are similar to Gd^{3+}. The EPR data in combination with photoluminescence measurements allows a direct attribution of optical properties to activator local structure. The observed blue luminescence here originates from Eu^{2+} centres in the amorphous phase. Thermal treatment at high temperatures promotes the $Eu^{3+} \rightarrow Eu^{2+}$ reduction efficiency and characteristic EPR spectra as well as additional luminescence bands can be observed.

THESES

- The temperature dependence of Gd^{3+} EPR fine structure parameter $|b_4|$ in ScF_3 crystal with negative thermal expansion is similar to cubic fluorides, which expand positively with temperature indicating the correlation of the EPR parameters to local atomic distances instead of crystallographic lattice constant.

- Gd^{3+} ions incorporate in the MeF_2 (Me = Ca, Ba, Sr) crystalline phase of oxyfluoride glass ceramics creating centres which can be described by EPR spectra parameters observed in the respective single crystals.

- When gadolinium substitutes similarly sized cations in glass ceramics with CaF_2 and SrF_2 crystallites mainly cubic Gd^{3+} centres are observed but due to a significant size mismatch of Ba^{2+} and Gd^{3+} ions trigonal symmetry BaF_2:Gd^{3+} centres can be observed.

- Most europium ions incorporate the SrF_2 crystalline phase of oxyfluoride glass ceramics in the 3+ valence state as the reduction to Eu^{2+} during thermal treatment is inefficient. By increasing the fluorine content in the composition it is possible to obtain self-reduced glass ceramics in which the blue luminescence mainly originates from Eu^{2+} in the amorphous phase.

REFERENCES

[1] V.I. Chizhik, Y.S. Chernyshev, A. V. Donets, V. V. Frolov, A. V. Komolkin, M.G. Shelyapina, Magnetic resonance and its applications, Spinger, 2014. doi:10.1007/978-3-319-05299-1.

[2] J.A. Weil, J.R. Bolton, Electron Paramagnetic Resonance, Wiley, 2007.

[3] M. Brustolon, E. Giamello, Electron Paramagnetic Resonance: A Practitioner's Toolkit, Wiley, 2008. doi:10.1002/9780470432235.

[4] G.R. Eaton, S.S. Eaton, D.P. Barr, R.T. Weber, Quantitative EPR, Springer, 2010.

[5] S. Stoll, A. Schweiger, EasySpin, a comprehensive software package for spectral simulation and analysis in EPR, J. Magn. Reson. 178 (2006) 42–55.

[6] V. Grachev, Visual-EPR, (n.d.). www.visual-epr.com.

[7] G.R. Hanson, K.E. Gates, C.J. Noble, M. Griffin, A. Mitchell, S. Benson, XSophe-Sophe-XeprView. A computer simulation software suite (v. 1.1.3) for the analysis of continuous wave EPR spectra, J. Inorg. Biochem. 98 (2004) 903–916. doi:10.1016/j.jinorgbio.2004.02.003.

[8] S. Stoll, CW-EPR Spectral Simulations: Solid State, Methods Enzymol. 563 (2015) 121–142. doi:10.1016/bs.mie.2015.06.003.

[9] S.A. Al'tshulter, B.M. Kozyrev, Electron Paramagnetic Resonance in Compounds of Transition Elements, Wiley, 1974.

[10] S. Graulis, D. Chateigner, R.T. Downs, A.F.T. Yokochi, M. Quirós, L. Lutterotti, et al., Crystallography Open Database – An open-access collection of crystal structures, J. Appl. Crystallogr. 42 (2009) 726–729. doi:10.1107/S0021889809016690.

[11] S. Gražulis, A. Daškevič, A. Merkys, D. Chateigner, L. Lutterotti, M. Quirós, et al., Crystallography Open Database (COD): An open-access collection of crystal structures and platform for world-wide collaboration, Nucleic Acids Res. 40 (2012) 420–427. doi:10.1093/nar/gkr900.

[12] R.T. Downs, M. Hall-Wallace, The American Mineralogist crystal structure database, Am. Mineral. 88 (2003) 247–250.

[13] K. Momma, F. Izumi, VESTA: A three-dimensional visualization system for electronic and structural analysis, J. Appl. Crystallogr. 41 (2008) 653–658. doi:10.1107/S0021889808012016.

[14] K. Momma, F. Izumi, VESTA 3 for three-dimensional visualization of crystal, volumetric and morphology data, J. Appl. Crystallogr. 44 (2011) 1272–1276. doi:10.1107/S0021889811038970.

[15] K. Smits, A. Sarakovskis, L. Grigorjeva, D. Millers, J. Grabis, The role of Nb in intensity increase of Er ion upconversion luminescence in zirconia, J. Appl. Phys. 115 (2014) 1–9. doi:10.1063/1.4882262.

[16] L. Grigorjeva, D. Millers, K. Smits, A. Zolotarjovs, Gas sensitive luminescence of ZnO coatings obtained by plazma electrolytic oxidation, Sensors Actuators, A Phys. 234 (2015) 290–293. doi:10.1016/j.sna.2015.09.018.

[17] K.S. Aleksandrov, N. V. Voronov, A.N. Vtyurin, A.S. Krylov, M.S. Molokeev, a. S. Oreshonkov, et al., Structure and lattice dynamics of the high-pressure phase in the ScF_3 crystal, Phys. Solid State. 53 (2011) 564–569. doi:10.1134/S1063783411030036.

[18] K.S. Aleksandrov, V.N. Voronov, A.N. Vtyurin, A.S. Krylov, M.S. Molokeev, M.S. Pavlovskiĭ, et al., Pressure-induced phase transition in the cubic ScF_3 crystal, Phys. Solid State. 51 (2009) 810–816. doi:10.1134/S1063783409040295.

[19] K.S. Aleksandrov, V.N. Voronov, A.N. Vtyurin, S. V. Goryainov, N.G. Zamkova, V.I. Zinenko, et al., Lattice dynamics and hydrostatic-pressure-induced phase transitions in ScF_3, J. Exp. Theor. Phys. 94 (2002) 977–984. doi:10.1134/1.1484991.

[20] B.K. Greve, K.L. Martin, P.L. Lee, P.J. Chupas, K.W. Chapman, A.P. Wilkinson, Pronounced Negative Thermal Expansion from a Simple Structure: Cubic ScF_3, J. Am. Chem. Soc. 132 (2010) 15496–15498. doi:10.1021/ja106711v.

[21] J.P. Attfield, Condensed-matter physics: A fresh twist on shrinking materials, Nature. 480 (2011) 465–466. doi:10.1038/480465a.

[22] P. Zhgun, D. Bocharov, S. Piskunov, A. Kuzmin, J. Purans, Electronic structure of cubic ScF_3 from first-principles calculations, (2012) 3–8. doi:10.1063/1.4959013.

[23] C.W. Li, X. Tang, J.A. Munoz, J.B. Keith, S.J. Tracy, D.L. Abernathy, et al., Structural relationship between negative thermal expansion and quartic anharmonicity of cubic ScF_3, Phys. Rev. Lett. 107 (2011) 1–5. doi:10.1103/PhysRevLett.107.195504.

[24] S. Piskunov, P.A. Zguns, D. Bocharov, A. Kuzmin, J. Purans, A. Kalinko, et al., Interpretation of unexpected behavior of infrared absorption spectra of ScF_3 beyond the quasiharmonic approximation, Phys. Rev. B – Condens. Matter Mater. Phys. 93 (2016). doi:10.1103/PhysRevB.93.214101.

[25] J. Chen, Q. Gao, A. Sanson, X. Jiang, Q. Huang, A. Carnera, et al., Tunable thermal expansion in framework materials through redox intercalation, Nat. Commun. 8 (2017) 14441. doi:10.1038/ncomms14441.

[26] C.R. Morelock, M.R. Suchomel, A.P. Wilkinson, A cautionary tale on the use of GE-7031 varnish: Low-temperature thermal expansion studies of ScF_3, J. Appl. Crystallogr. 46 (2013) 823–825. doi:10.1107/S0021889813005955.

[27] S.U. Handunkanda, E.B. Curry, V. Voronov, A.H. Said, G.G. Guzman-Verri, R.T. Brierley, et al., Large isotropic negative thermal expansion above a structural quantum phase transition, Phys. Rev. B – Condens. Matter Mater. Phys. 92 (2015) 1–6. doi:10.1103/PhysRevB.92.134101.

[28] L.S. Starostina, B.N. Grechushnikov, V.F. Koryagin, Paramagnetic Ions Gd^{3+}, Mn^{2+} in ScF_3 Crystal, Fiz. Tverd. Tela. 14 (1972) 3480–3483.

[29] Y. Vaills, J.Y. Buzare, EPR studies of Gd^{3+} centres in the cubic phase of $CsCaCl_3$ and $CsPbCl_3$, J. Phys. Chem. Solids. 48 (1987) 363–370. doi:10.1016/0022-3697(87)90095-3.

[30] M. Arakawa, H. Ebisu, T. Yosida, K. Horai, Electron Paramagnetic Resonance Studies of Gd^{3+} un $KZnF_3$ and $KCdF_3$, J. Phys. Soc. Japan. 46 (1979) 1483–1487.

[31] J.Y. Buzare, M. Fayet-Bonnel, J.C. Fayet, EPR investigations of the superhyperfine interaction and of the zero-field splittings for cubic and tetragonal Gd^{3+} centres at sixfold coordinated sites in AMF_3 crystals, J. Phys. C Solid State Phys. 14 (1981).

[32] M. Arakawa, H. Ebisu, H. Takeuchi, Electron paramagnetic resonance study of Gd^{3+} centres in cubic and hexagonal perovskite $RbZnF_3$ crystals, J. Physics-Condensed Matter. 9 (1997) 5193–5204. doi:10.1088/0953-8984/9/24/016.

[33] T. Rewaj, M. Krupski, J. Kuriata, J.Y. Buzare, Temperature and hydrostatic pressure dependences of the b_4^0 spin-Hamiltonian parameter for Gd^{3+} in fluoroperovskite single crystals, J. Phys. Condens. Matter. 4 (1992) 9909–9918.

[34] P. Fornasini, N. Abd el All, S.I. Ahmed, A. Sanson, M. Vaccari, Negative thermal expansion and local dynamics, J. Phys. Conf. Ser. 190 (2009) 12025. doi:10.1088/1742-6596/190/1/012025.

[35] A.A. Kaminskii, A. V. Butashin, J. Hulliger, P. Egger, S.N. Bagayev, H.J.. Eichler, et al., New anisotropic rare earth fluorides BaR2F8 (R=Y, Dy–Lu): growth and characterization, J. Alloys Compd. 275–277 (1998) 442–446. doi:10.1016/S0925-8388(98)00364-8.

[36] A.A. Kaminskii, O. Lux, J. Hanuza, H. Rhee, H.J. Eichler, J. Zhang, et al., Monoclinic β-BaY_2F_8 —a novel crystal simultaneously active for SRS and Ln^{3+} -ion lasing, Laser Phys. 25 (2015) 15801. doi:10.1088/1054-660X/25/1/015801.

[37] W. Liu, C. Li, J. Xu, Y. Zhou, H. Xie, M. Gao, et al., Growth and spectral properties of Tm:BaY_2F_8 crystals with different Tm^{3+} concentration, Russ. J. Phys. Chem. A. 90 (2016) 252–256. doi:10.1134/S0036024416010076.

[38] D. Pabœuf, O. Mhibik, F. Bretenaker, P. Goldner, D. Parisi, M. Tonelli, Diode-pumped Pr:BaY_2F_8 continuous-wave orange laser., Opt. Lett. 36 (2011) 280–282. doi:10.1364/OL.36.000280.

[39] A. Boccolini, R. Faoro, E. Favilla, S. Veronesi, M. Tonelli, BaY_2F_8 doped with Er^{3+}: An upconverter material for photovoltaic application, J. Appl. Phys. 114 (2013). doi:10.1063/1.4817171.

[40] A. Boccolini, E. Favilla, M. Tonelli, B.S. Richards, R.R. Thomson, Highly efficient upconversion in Er^{3+} doped BaY_2F_8 single crystals: dependence of quantum yield on excitation wavelength and thickness, Opt. Express. 23 (2015) A903. doi:10.1364/OE.23.00A903.

[41] S. Fischer, E. Favilla, M. Tonelli, J.C. Goldschmidt, Record efficient upconverter solar cell devices with optimized bifacial silicon solar cells and monocrystalline BaY_2F_8:30% Er^{3+} upconverter, Sol. Energy Mater. Sol. Cells. 136 (2015) 127–134. doi:10.1016/j.solmat.2014.12.023.

[42] J. Pejchal, M. Nikl, K. Fukuda, N. Kawaguchi, T. Yanagida, Y. Yokota, et al., Doubly doped BaY_2F_8:Er,Nd VUV scintillator, Radiat. Meas. 45 (2010) 265–267. doi:10.1016/j.radmeas.2009.10.017.

[43] G. Amoretti, D.C. Giori, V. Varacca, EPR of Gd^{3+} in a Single Crystal of Thorium disulfide (ThS_2), Z. Naturforsch. 36a (1981) 1163–1168.

[44] P.P. Fedorov, A.A. Luginina, A.I. Popov, Transparent oxyfluoride glass ceramics, J. Fluor. Chem. 172 (2015) 22–50. doi:10.1016/j.jfluchem.2015.01.009.

[45] A.J. Stevenson, H. Serier-Brault, P. Gredin, M. Mortier, Fluoride materials for optical applications: Single crystals, ceramics, glasses, and glass-ceramics, J. Fluor. Chem. 132 (2011) 1165–1173. doi:10.1016/j.jfluchem.2011.07.017.

[46] M. Mohapatra, R.K. Mishra, C.P. Kaushik, S. V. Godbole, Photoluminescence investigations of rare earth (Eu and Gd) incorporated nuclear waste glass, Phys. B Condens. Matter. 405 (2010) 4790–4795. doi:10.1016/j.physb.2010.09.003.

[47] M. Mohapatra, B. Rajeswari, N.S. Hon, R.M. Kadam, M.S. Keskar, V. Natarajan, An electron spin resonance and photoluminescence investigation of the effect of annealing temperature on Gd-doped $La_2Zr_2O_7$ nano-ceramics, Ceram. Int. 41 (2015) 8761–8767. doi:10.1016/j.ceramint.2015.03.099.

[48] M. Bosca, L. Pop, L. Bolundut, N. Tothazan, G. Borodi, I. Vida-Simiti, et al., Effects of Gd^{3+}: Ag co-doping on structural and magnetic properties of lead tellurite glass ceramics, Ceram. Int. 42 (2016) 1169–1176. doi:10.1016/j.ceramint.2015.09.047.

[49] P. Pascuta, E. Culea, Effect of gadolinium ions on the structure and magnetic properties of zinc-borate glasses and glass ceramics, J. Mater. Sci. 47 (2012) 2345–2351. doi:10.1007/s10853-011-6051-1.

[50] D. Furniss, E.A. Harris, D.B. Hollis, EPR of Gd^{3+} and Eu^{2+} in fluorozirconate glasses, J. Phys. C Solid State Phys. 20 (1987) L147–L150. doi:10.1088/0022-3719/20/10/002.

[51] S. Schweizer, G. Corradi, A. Edgar, J.-M. Spaeth, EPR of Eu^{2+} in $BaBr_2$ crystals and fluorobromozirconate glass ceramics, J. Phys. Condens. Matter. 13 (2001) 2331–2338. doi:10.1088/0953-8984/13/10/323.

[52] C.M. Brodbeck, L.E. Iton, The EPR spectra of Gd^{3+} and Eu^{2+} in glassy systems, J. Chem. Phys. 83 (1985) 4285. doi:10.1063/1.449041.

[53] C. Legein, J.Y. Buzaré, G. Silly, C. Jacoboni, The local field distribution of Gd^{3+} in transition metal fluoride glasses investigated by electron paramagnetic resonance, J. Phys. Condens. Matter. 8 (1996) 4339–4350. doi:10.1088/0953-8984/8/23/023.

[54] J. Sierro, Paramagnetic resonance of Gd^{3+} in SrF_2 and BaF_2, Phys. Lett. 4 (1963) 178–180. doi:10.1093/jicru/ndp028.

[55] W.-Q. Yang, Y. Zhang, Y. Lin, W.-C. Zheng, Spin-Hamiltonian parameters for the tetragonal centers in CaF_2 and SrF_2 crystals, J. Magn. Reson. 227 (2013) 62–65. doi:10.1016/j.jmr.2012.12.003.

[56] C. Yang, S. Lee, A.J. Bevolo, Investigations of the weak trigonal Gd^{3+} ESR center in alkaline-earth fluoride crystals, Phys. Rev. B. 13 (1976) 2762–2767.

[57] S. Lee, C. Yang, A.J. Bevolo, Investigations of the new trigonal Gd^{3+} ESR center produced in irradiated alkaline-earth fluoride crystals, Phys. Rev. B. 10 (1974) 4515–4522.

[58] C. Yang, S. Lee, A.J. Bevolo, Investigations of two trigonal (T_1 and T_2) Gd^{3+} ESR centers in treated alkaline-earth-fluoride crystals, Phys. Rev. B. 12 (1975) 4687–4694.

[59] S. Ouyang, W. Zhang, Z. Zhang, Y. Zhang, Near-Green-Emitting Tb^{3+}-Doped Transparent Glass Ceramics Containing Ba_2LaF_7 Nanocrystals for Application in White Light-Emitting Diodes, J. Appl. Spectrosc. 83 (2016) 277–282. doi:10.1007/s10812-016-0281-6.

[60] H. Jin, Z. Mo, X. Zhang, L. Yuan, M. Yan, L. Li, Luminescent properties of Eu^{3+}-doped glass ceramics containing $BaCl_2$ nanocrystals under NUV excitation for White LED, J. Lumin. 175 (2016) 187–192. doi:10.1016/j.jlumin.2016.03.002.

[61] M. Kemere, J. Sperga, U. Rogulis, G. Krieke, J. Grube, Luminescence properties of Eu, RE^{3+} (RE = Dy,Sm,Tb) co-doped oxyfluoride glasses and glass–ceramics, J. Lumin. 181 (2017) 25–30. doi:10.1016/j.jlumin.2016.08.062.

[62] C.R. Li, S.F. Li, Y.Y. Guo, X.Y. Zhou, J.C. Sun, Y. Song, et al., White light emission of Dy^{3+}-doped and Dy^{3+}:Yb^{3+}-codoped oxyfluoride glass ceramics under 388-nm excitation, 340 (2015). doi:10.1080/09500340.2015.1061060.

[63] L.Q. Yao, G.H. Chen, H.J. Zhong, S.C. Cui, F. Li, J.Y. Gan, Enhanced Luminescent Properties in Tm^{3+}/ Dy^{3+} Transparent Phosphate Glass Ceramic, in: MATEC Web Conf., 2016.

[64] Z. Zhang, Y. Zhang, Z. Feng, W. Cheng, H. Xia, X. Zhang, Luminescent properties of Ce^{3+}/ Tb^{3+} co-doped glass ceramics containing YPO_4 nanocrystals for W-LEDs, J. Rare Earths. 34 (2016) 464–469. doi:10.1016/S1002-0721(16)60050-9.

[65] D. Chen, W. Xiang, X. Liang, J. Zhong, H. Yu, M. Ding, et al., Advances in transparent glass–ceramic phosphors for white light-emitting diodes—A review, J. Eur. Ceram. Soc. 35 (2015) 859–869. doi:10.1016/j.jeurceramsoc.2014.10.002.

[66] P.P. Fedorov, A.A. Luginina, A.I. Popov, Transparent oxyfluoride glass ceramics, J. Fluor. Chem. 172 (2015) 22–50. doi:10.1016/j.jfluchem.2015.01.009.

[67] C.M. Brodbeck, R.R. Bukrey, Model calculations for the coordination of Fe^{3+} and Mn^{2+} ions in oxide glasses, Phys. Rev. B. 24 (1981) 2334–2342.

[68] R.S. Title, The cubic field splitting of the Eu^{++} EPR spectrum in the alkaline earth fluorides, Phys. Lett. 6 (1963) 13–14.

[69] D.S. Jo, Y. Luo, K. Senthil, K. Toda, B.S. Kim, T. Masaki, et al., Synthesis and photoluminescence properties of new $NaAlSiO_4$:Eu^{2+} phosphors for near-UV white LED applications, Opt. Mater. (Amst). 34 (2012) 696–699. doi:10.1016/j.optmat.2011.10.004.

[70] Y. Guo, X. Yu, J. Liu, X. Yang, Photoluminescence of Eu^{2+}-activated $Na_{1-x}Al_{1-x}Si_{1+x}O_4$ upon UV excitation, J. Rare Earths. 28 (2010) 34–36. doi:10.1016/S1002-0721(09)60045-4.

[71] J. Chen, Y. Liu, H. Liu, H. Ding, M. Fang, Z. Huang, Tunable $SrAl_2Si_2O_8$: Eu phosphor prepared in air via valence state-controlled means, Opt. Mater. (Amst). 42 (2015) 80–86. doi:10.1016/j.optmat.2014.12.023.

[72] Z. Wang, Y. Wang, P. Zhang, X. Fan, G. Qian, Tunable afterglow color in Eu^{2+} and Dy^{3+} co-activated alkaline earth feldspar solid solutions phosphors, J. Lumin. 124 (2007) 140–142. doi:10.1016/j.jlumin.2006.02.015.

[73] M. Bau, Rare-Earth Element Mobility During Hydrothermal and Metamorphic Fluid Rock Interaction and the Significance of the Oxidation-State of Europium, Chem. Geol. 93 (1991) 219–230. doi:10.1016/0009-2541(91)90115-8.

[74] Z. Lin, H. Zeng, Y. Yang, X. Liang, G. Chen, L. Sun, The effect of fluorine anions on the luminescent properties of Eu-Doped oxyfluoride aluminosilicate glasses, J. Am. Ceram. Soc. 93 (2010) 3095–3098. doi:10.1111/j.1551-2916.2010.04067.x.

[75] R.R. Reddy, Y. Nazeer Ahammed, K. Rama Gopal, P. Abdul Azeem, T.V.R. Rao, Correlation between optical basicity, electronegativity and electronic polarizability for some oxides and oxysalts, Opt. Mater. (Amst). 12 (1999) 425–428. doi:10.1016/S0925-3467(98)00083-4.

[76] C. Zhu, D. Wu, Y. Zhang, M. Zhang, Y. Yue, Composition dependence of the optical and structural properties of Eu-doped oxyfluoride glasses, J. Alloys Compd. 632 (2015) 291–295. doi:10.1016/j.jallcom.2015.01.207.

AUTHOR'S PUBLICATIONS

Related to this work

- A. Antuzevics, U. Rogulis, A. Fedotovs, Dz. Berzins, V. N. Voronov, J. Purans, EPR study of Gd^{3+} local structure in ScF_3 crystal with negative thermal expansion coefficient, Phys. Scr. 90 (2015) 115801 doi: 10.1088/0031-8949/90/11/115801 (Scopus, WoS, IF = 1,28)
- A. Fedotovs, A. Antuzevics, U. Rogulis, M. Kemere, R. Ignatans, Electron paramagnetic resonance and magnetic circular dichroism of Gd^{3+} ions in oxyfluoride glass-ceramics containing CaF_2 nanocrystals, J. Non-Cryst. Solids 429 (2015) 118-121, doi: 10.1016/j.jnoncrysol.2015.08.036 (Scopus, WoS, IF = 2,124)
- A. Antuzevics, M. Kemere, R. Ignatans, Local structure of gadolinium in oxyfluoride glass matrices containing SrF_2 and BaF_2 crystallites, J. Non-Cryst. Solids 449 (2016) doi: 10.1016/j.jnoncrysol.2016.07.015 (Scopus, WoS, IF = 2,124)
- A. Antuzevics, M. Kemere, G. Krieke, R. Ignatans, Electron paramagnetic resonance and photoluminescence investigation of europium local structure in oxyfluoride glass ceramics containing SrF_2 nanocrystals, Opt. Mater. 72 (2017) doi: 10.1016/j.optmat.2017.07.024 (Scopus, WoS, IF = 2,238)
- A. Antuzevics, U. Rogulis, A. Fedotovs, A. Popov, Crystalline phase detection in glass ceramics by EPR spectroscopy, Low Temp. Phys. (accepted for publication) (Scopus, WoS, IF = 0,804)

Other publications

- A. Antuzevics, U. Rogulis, A. Fedotovs, EPR spectrum angular dependences in $LiYF_4$ crystal, Latv. J. Phys. Tech. Sci. 6 (2012) 115801 doi: 10.2478/v10047-012-0034-0 (Scopus)
- A. N. Trukhin, A. Antuzevics, K. Golant, D. L Griscom, Luminescence of phosphorus doped silica glass, J. Non-Cryst. Solids 462 (2017) 10-16 doi: 10.1016/j.jnoncrysol.2017.02.002 (Scopus, WoS, IF = 2,124)
- P. Lesnicenoks, L. Grinberga, L. Jekabsons, A. Antuzevics, A. Berzina, M. Knite, G. Taurins, S. Varnagiris, J. Kleperis, Nanostructured carbon materials for hydrogen energetics, Adv. Mater. Lett. 8 (2017) 518-523 doi: 10.5185/amlett.2016.7088 (IF = 1,46)
- U. Rogulis, A. Fedotovs, A. Antuzevics, Dz. Berzins, Ya. Zhydachevskyy, D. Sugak, Optical detection of paramagnetic centres in activated oxyfluoride glass-ceramics, Acta. Phys. Pol. A (accepted for publication) (Scopus, WoS, IF = 0,459)

CONTRIBUTIONS AT SCIENTIFIC CONFERENCES

Local conferences

- A. Fedotovs, A. Antuzevičs, M. Ķemere, Dz. Bērziņš, Paramagnētiskās zondes oksifluorīdu stikla keramiku struktūras pētījumiem, LU ISSP 31st Scientific Conference (2015).
- A. Antuzevičs, M. Ķemere, E. Elsts, R. Ignatāns, Gd^{3+} lokālā struktūra CaF_2, SrF_2, BaF_2 un $NaLaF_4$ kristalītus saturošās stikla matricās, LU ISSP 32nd Scientific Conference (2016).
- A. Antuzevičs, A. Fedotovs, Dz. Bērziņš, U. Rogulis, R. Ignatāns, S. Baldochi. Magnētiskās rezonanses spektroskopijas pētījumi BaY_2F_8 kristālā, LU ISSP 32nd Scientific Conference (2016).
- A. Antuzevičs, M. Ķemere, R. Ignatāns, S-stāvokļa jonu struktūra un īpašības stiklu keramikās, LU ISSP 33rd Scientific Conference (2017)
- A. Antuzevičs, A. Fedotovs, Dz. Bērziņš, U. Rogulis, R. Ignatāns, S. Baldochi, Gd^{3+} un V_K centrs BaY_2F_8 kristālā, LU ISSP 33rd Scientific Conference (2017)
- G. Priedītis, M. Ķemere, A. Antuzevičs, U. Rogulis, Ar eiropiju un gadolīniju aktivētu oksifluorīdu stikla keramiku fotoluminiscence, LU ISSP 33rd Scientific Conference (2017)
- U. Rogulis, A. Fedotovs, A. Antuzevičs, Dz. Bērziņš, Paramagnētisku centru optiskā detekcija aktivētās oksifluorīdu stikla keramikās, LU ISSP 33rd Scientific Conference (2017)

International conferences

- A. Antuzevics, U. Rogulis, A. Fedotovs, Dz. Berzins, J. Purans, Electron paramagnetic resonance study of point defects in ScF_3, Inter-Academia 2014, Riga, Latvia (2014)
- A. Antuzevics, U. Rogulis, J. Purans, A. Fedotovs, Dz. Berzins, EPR spectra of ScF_3, RCBJSF-2014-FM&NT, Riga, Latvia (2014)
- A. Antuzevics, U. Rogulis, J. Purans, EPR investigation of Gd^{3+} local structure in ScF_3, Developments in Optics and Communications, Riga, Latvia (2015)
- A. Antuzevics, A. Fedotovs, U. Rogulis, M. Kemere, Paramagnetic probes for nano-crystalline phase detection in oxyfluoride glass ceramics, EuroNanoForum 2015, Riga, Latvia (2015)
- A. Antuzevics, A. Fedotovs, U. Rogulis, M. Kemere, EPR study of oxyfluoride glass ceramics containing Gd^{3+} ions, LUMDETR 2015, Tartu, Estonia (2015)

- A. Antuzevics, M. Kemere, R. Ignatans, Electron paramagnetic resonance study of Gd^{3+} ions in oxyfluoride glass ceramics, Open Readings 2016, Vilnius, Lithuania (2016)
- A. Antuzevics, M. Kemere, R. Ignatans, Structure of Gd^{3+} ions in oxyfluoride glass ceramics containing fluorite crystallites, Developments in Optics and Communications, Riga, Latvia (2016)
- A. Antuzevics, M. Kemere, R. Ignatans, Combined white light emission of europium ions in glass ceramics, Developments in Optics and Communications, Riga, Latvia (2017)
- A. Antuzevics, M. Kemere, R. Ignatans, EPR and photoluminescence investigations of europium local structure in glass ceramics, Functional materials and Nanotechnologies 2017, Tartu, Estonia (2017)

ACKNOWLEDGEMENTS

I would like to express a sincere gratitude to my supervisor prof. Uldis Rogulis for the given opportunity to start my scientific career in the Laboratory of Magnetic Resonance Spectroscopy as well as the invested time sharing knowledge, experience and valuable advice. Thanks for an especially fruitful collaboration in research to Meldra Kemere, Guna Krieke, Reinis Ignatans and Krisjanis Smits and to Andris Fedotovs for assistance in technical difficulties and a friendly motivation during other struggles. A significant contribution to the results in this thesis comes from Dr.habil.phys. Juris Purans who stimulated a more thorough analysis of the experimental results.

The deepest gratitude to my loving parents for the never-ending support in studies and life and, of course, to Ilze and Ricards…

This work was supported financially by Scientific Research Projects for Students and Young Researchers Nr. SJZ2015/1 and SJZ/2016/3 realized at the institute of Solid State Physics, University of Latvia, ERAF project Nr.2014/0047/2DP/2.1.1.1.0/14/APIA/VIAA/007 and State research program IMIS-2.